Supplementary Information

Lithography-Free Patterning of $SrTiO_3$ -based Two-Dimensional Electron Gases using Direct Atomic Layer Processing

Anshu Gupta[1], Karolis Parfeniukas[2], Amit Chanda[1], Thor Hvid-Olsen[1], Mira Baraket[2], Maksym Plakhotnyuk[2], Kasper S. Pedersen[3], Felix Trier[1,*]

[1]Department of Energy Conversion and Storage, Technical University of Denmark, Kgs. Lyngby, Denmark

[2]ATLANT 3D, Taastrup, Denmark

[3]Department of Chemistry, Technical University of Denmark, Kgs. Lyngby, Denmark

Email: fetri@dtu.dk

1. Extended structural information

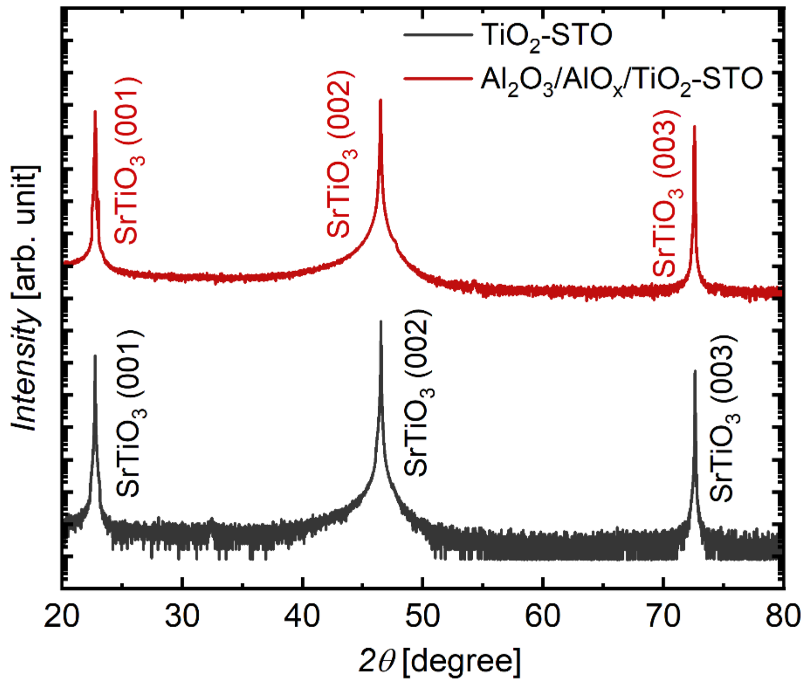

Figure S1. (a) X-ray diffraction (XRD) pattern of before deposition (TiO_2-STO) and after deposition ($Al_2O_3/AlO_x/TiO_2$-STO) at room temperature using a Rigaku SmartLab diffractometer

Alt text: XRD patterns comparing TiO_2-STO substrate before deposition and $Al_2O_3/AlO_x/TiO_2$-STO heterostructure after deposition, showing characteristic diffraction peaks and structural changes.

2. Extended morphological information

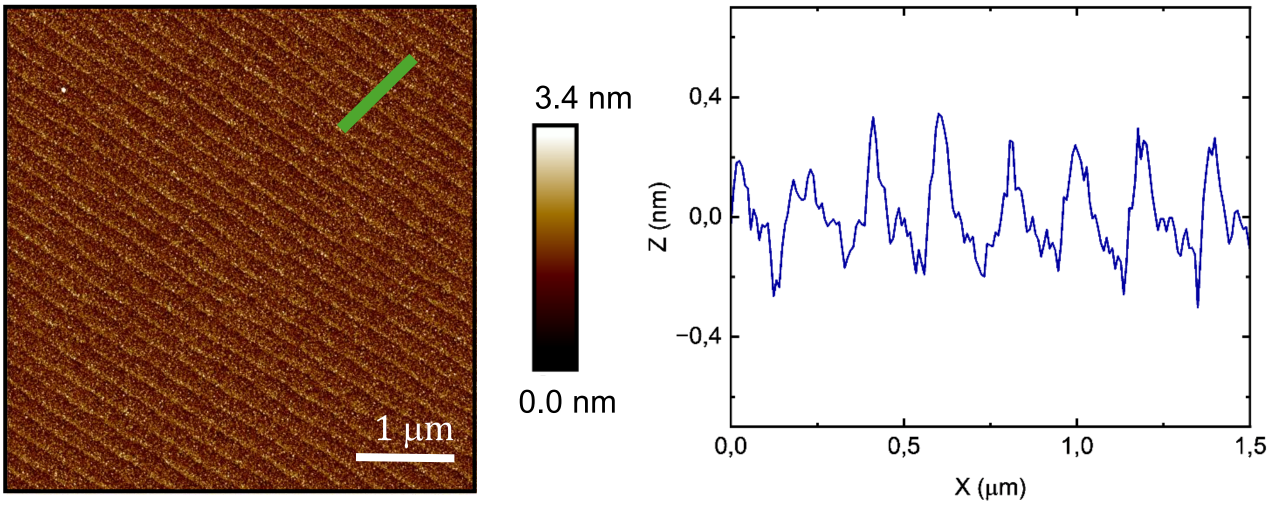

Figure S2. Atomic force microscopy image of the TiO_2-STO substrate showing root mean square (RMS) roughness approximately ≈ 0.3 nm. The image on the right highlights well-defined step–terrace features with a step height of about 0.4 nm.

Alt text: AFM images of TiO_2-STO substrate showing smooth surface morphology with low roughness and clear step-terrace structures.

3. Fitting results of the temperature dependent sheet resistance

	Parameters	$Al_2O_3/AlO_x/TiO_2$-STO
Low Temperature Fitting (2 K ≤ *T* ≤ 25 K)	$\boldsymbol{R_0}$ **(Ω/sq)**	617.78 ± 6.02
	$\boldsymbol{R_{inel}}$ $(\boldsymbol{\Omega.K^{-n}/sq})$	0.123 ± 0.002
	$\boldsymbol{n}$	2
	$\boldsymbol{R_{Kondo}}$ **(Ω/sq)**	49.13 ±2.1
	$\boldsymbol{T_K}$ **(K)**	13.99 ± 1.5
	$\boldsymbol{R^2}$ **value of the fit**	0.9968

Table S1. List of parameters obtained by fitting the R_s(T) data for $Al_2O_3/AlO_x/TiO_2$-STO heterostructure.

Alt text: Table listing fitting parameters extracted from temperature-dependent sheet resistance measurements of the $Al_2O_3/AlO_x/TiO_2$-STO heterostructure.

4. Optical microscopy images of $Al_2O_3/AlO_x/TiO_2$-$SrTiO_3$ patterned heterostructures and electrical measurement configuration.

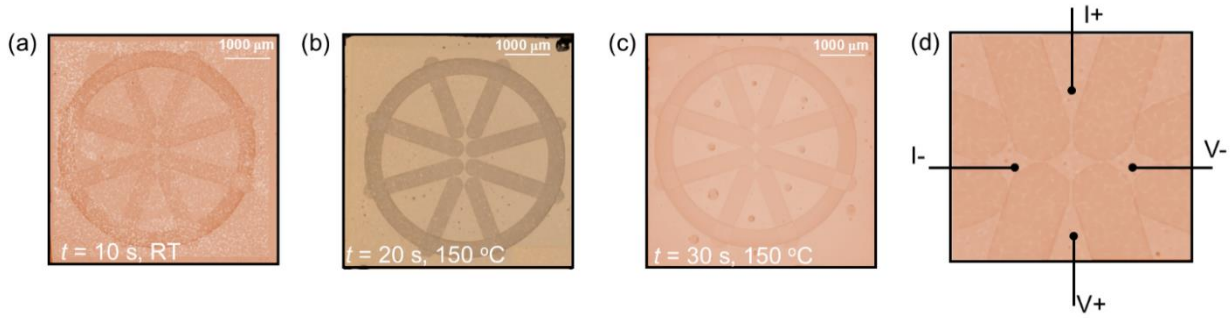

Figure S4: (a-c) Optical microscope images showing the $Al_2O_3/AlO_x/TiO_2$-$SrTiO_3$ heterostructure (STO) substrate after deposition. AlO_x deposition for (a) 10 s at room temperature 20 ºC, (b) 20 s at 150 ºC, and (c) 30 s at 150 ºC. The scale bar corresponds to 1000 µm. (d) Schematic representation of the four-terminal electrical measurement configuration used for transport measurements, showing current (I+/I-) and voltage (V+/V-) contact arrangement.

Alt text: Optical microscope images of patterned $Al_2O_3/AlO_x/TiO_2$-$SrTiO_3$ heterostructures and transport measurement geometry. Panels (a-c) show circular TiO_2patterned regions on STO substrates after AlO_x deposition under different conditions: (a) 10 s deposition at room temperature, (b) 20 s deposition at 150 °C, and (c) 30 s deposition at 150 °C. Each image includes a 1000 µm scale bar. Panel (d) illustrates the four-terminal measurement configuration, with current applied through the contacts (I+ and I-) and voltage measured across the contacts (V+ and V-).

5. Room-temperature (300 K) transport parameters of $Al_2O_3/AlO_x/TiO_2$-$SrTiO_3$

The table summarizes room-temperature (300 K) transport parameters of the $Al_2O_3/AlO_x/TiO_2$-$SrTiO_3$ heterostructures as a function of Al deposition time and growth temperature. The sheet resistance (R_s), carrier concentration (n_s), and Hall mobility (μ) show a strong dependence on deposition conditions, indicating tunable interfacial electronic reconstruction and carrier scattering with Al thickness and growth temperature.

t (s)	R_s (kΩ/sq.)	n_s (cm^{-2})	μ (cm^2/Vs)
10 s, T_G = 150 °C	12.0	7.7×10^{13}	6.7
20 s, T_G = 150 °C	27.8	5.7×10^{14}	0.4
30 s, T_G = 150 °C	28.6	2.0×10^{14}	1.0
10 s, T_G = 20 °C	50.4	1.3×10^{14}	0.9

Table S2: Room-temperature (300 K) transport parameters of $Al_2O_3/AlO_x/TiO_2$-$SrTiO_3$ heterostructures for different Al deposition times (t) and growth temperatures (T_G). The sheet resistance (R_s), sheet carrier density (n_s), and Hall mobility (μ) are extracted from Hall measurements, showing systematic variation with deposition conditions.

Alt text: Room-temperature Hall transport parameters of $Al_2O_3/AlO_x/TiO_2$-$SrTiO_3$ heterostructures, including sheet resistance, carrier density, and mobility as a function of Al deposition time and growth temperature.

6. Sheet resistance R_s dependence on the Al deposition time

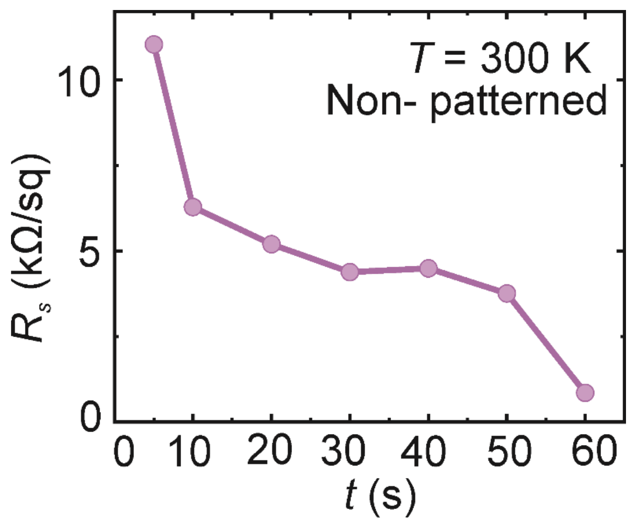

Figure S5: Sheet resistance R_s dependence on the Al deposition time at T = 300 K. The data were acquired for samples without TiO_2 patterning.

Alt text: Figure presents the dependence of R_s measured at 300 K as a function of Al deposition time during sputtering of samples prepared without TiO_2 mask. R_s decreases systematically with increasing deposition time, corresponding to a greater Al thickness. Specifically, R_s decreases from approximately ≈20.27 kΩ/sq. for a 5 s deposition to about ≈1.55 kΩ/sq. for a 60 s deposition.

7. Symmetrization and antisymmetrization of magnetotransport data

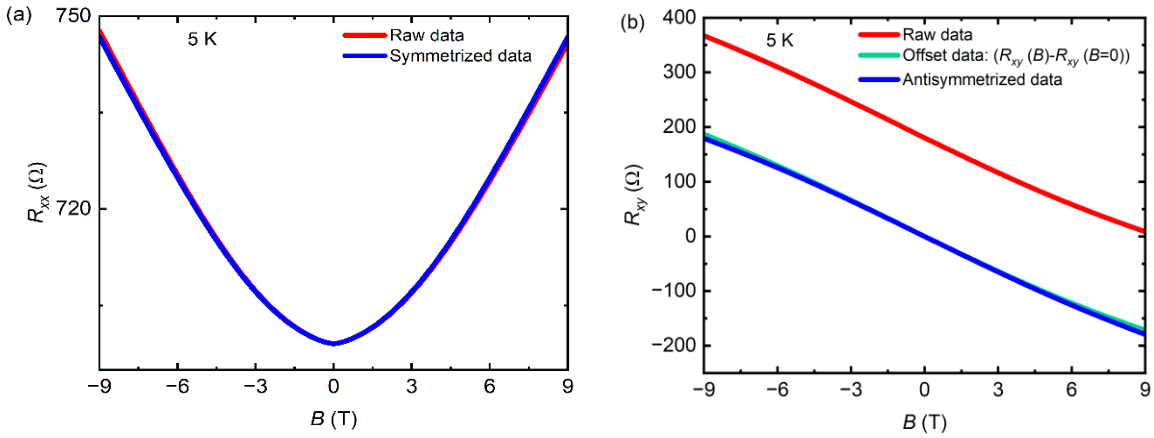

Figure S6: (a) Raw longitudinal resistance $R_{xx}(B)$ and symmetrized magnetoresistance obtained (b) Raw Hall resistance $R_{xy}(B)$, offset Hall resistance and antisymmetrized Hall resistance extracted. The procedure removes the contribution arising from contact misalignment and isolates the longitudinal and transverse transport components.

Alt text: The left panel presents symmetrized magnetoresistance as a function of magnetic field at low temperature, showing a symmetric field dependence. The right panel shows antisymmetrized Hall resistance versus magnetic field, after removing symmetric contributions, and the offset Hall resistance obtained by subtracting the raw Hall data $R_{xy}(B)$ from Hall resistance at zero magnetic field ($R_{xy}(B = 0)$).

8. Time-Dependent Evolution of Electrical Transport Properties

We have compared the transport properties measured shortly after growth with those obtained now after storage time in a 1 bar N_2 environment for over 250 days. We did not observe any significant long-term degradation or systematic evaluation of the transport properties in our sample. As shown here, the sheet resistance at 5 K changes from ≈ 699 Ω/sq. (time = 0 days) to 667 Ω/sq. (time = 250 days), while at 300 K it changes from approximately 11.5 kΩ/sq. to 12.0 kΩ/sq. The corresponding Hall analysis shows only minor variations in carrier density and mobility. At 5 K, the mobility changes from ≈ 734.6 $cm^2V^{-1}s^{-1}$ (time = 0 days) to 895.4 $cm^2V^{-1}s^{-1}$ (time = 250 days), while the total carrier density n_s changes from ≈ 5.5 x 10^{13} cm^{-2} (time =

0 days) to 6.2 x 10^{13} cm^{-2} (time = 250 days). In our case, the conducting interface is stabilized by the 33 nm thick Al_2O_3 capping layer, resulting in stable transport properties over time.

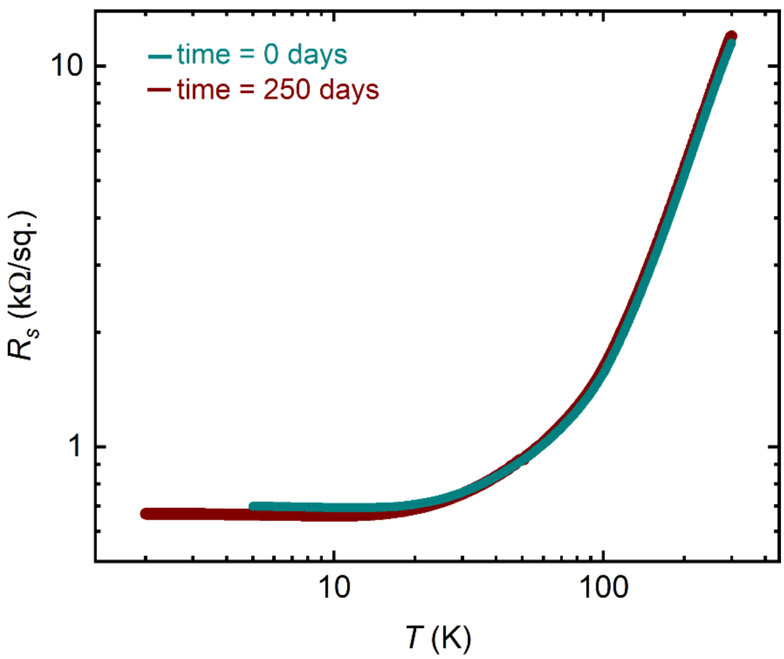

Figure S7: Temperature dependence of sheet resistance, R_s(T), measured between 5 K and 300 K immediately after growth (t = 0 days) and after 250 days of aging, showing the evolution of transport behavior over time.

Alt text: Temperature-dependent sheet resistance of the sample measured from 5 K to 300 K immediately after growth and after 250 days of storage, showing similar transport behavior over time.